THE JOURNAL OF PHYSICAL CHEMISTRY C

Article

pubs.acs.org/JPCC

Thiolate-Bonded Self-Assembled Monolayers on Ni(111): Bonding Strength, Structure, and Stability

F. Blobner,[†] P. N. Abufager,[‡] R. Han,[†] J. Bauer,[†] D. A. Duncan,[†] R. J. Maurer,[§] K. Reuter,*[,§] P. Feulner,[†] and F. Allegretti*[,†]

[†]Physik-Department E20, Technische Universität München, James-Franck-str. 1, D-85748 Garching, Germany

[‡]Instituto de Física de Rosario, Consejo Nacional de Investigaciones Científicas y Técnicas (CONICET) and Universidad Nacional de Rosario, Av. Pellegrini 250, 2000 Rosario, Argentina

[§]Department Chemie, Technische Universität München, Lichtenbergstr. 4, D-85747 Garching, Germany

Supporting Information

ABSTRACT: Self-assembled monolayers (SAMs) grown on surfaces of ferromagnetic metals have attracted increasing attention as they can act as corrosion inhibitors on easily oxidizable transition metals and are potentially relevant for application in spintronics. We have performed a model study of aromatic thiol SAMs grown on atomically flat Ni(111) by means of synchrotron-based X-ray photoelectron spectroscopy, X-ray absorption spectroscopy, and density functional theory. Our analysis demonstrates that well-defined bonding through the sulfur headgroup of the molecules (thiolate bonding) can be established at 200 K. However, the bonding configuration is metastable: breaking of the C−S bond and subsequent chemisorption of both fragments on the Ni surface decreases the total energy. The low activation barrier for C−S dissociation hampers the formation of room-temperature-stable monolayers. In addition, we show that end groups with a strong affinity to the nickel substrate can severely modify the global pattern of interaction of the thiol molecules with the surface upon adsorption.

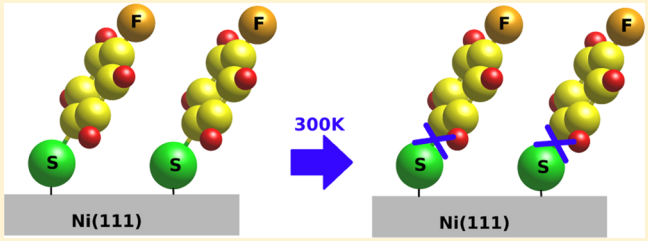

1. INTRODUCTION

The formation and patterning of self-assembled monolayers (SAMs) covalently bonded to well-defined metal surfaces continues to attract the interest of the scientific community after several decades of research, due to the high potential of these systems in diverse areas of technology including molecular electronics,[1−3] biomedical devices and drug delivery,[4,5] and nanotechnology.[2,6] In particular, thiolate-bonded SAMs on gold surfaces have been frequently regarded as prototypical systems thanks to the high affinity of the sulfur headgroup to the substrate, the robustness of the chemisorptive bond, which leads to SAMs that are stable at room temperature, and the ease of preparation by wet-chemical routes (e.g., from solution).[7] Surprisingly, despite extensive investigation of these systems in highly controlled ultrahigh vacuum (UHV) conditions by means of a plethora of surface science tools, the details of the interaction of thiols with gold, and especially with the Au(111) surface, still remain a matter of controversy.[3,8−13] This might partly explain why the formation of thiol SAMs on the more reactive surfaces of d transition metals such as Ni, Co, Pt, and Pd has received, comparatively, much less attention. In fact, for these metals the demand of preparing oxide-free surfaces in an ambient environment cannot be easily met,[14−18] thus rendering even more complicated, from the experimental point of view, the characterization of the thiol−metal interaction and the insight into the structure−properties relationship of the resulting SAMs.

However, renewed interest in SAMs deposited onto substrates and electrodes of 3d ferromagnetic metals (specifically Ni, Co, and Fe) has arisen in recent years[15,16,19] and is expected to grow steadily due to the crucial role envisaged for organic layers in molecular spintronics.[20−23] The latter discipline relies on the ability to manipulate the electron spin in organic molecular materials, which can provide a chemical route for tailoring the magnetic response in electronic devices.[24] In this context, the spin-dependent transport through aromatic dithiol molecules sandwiched between magnetic Ni contacts has been considered by theoretical investigations from different research groups,[20,24−26] and large magnetoresistance ratios have been predicted when switching the magnetization of the two Ni electrodes from parallel to antiparallel. The bias-dependent magnetoresistance has been attributed to a spin-selective coupling of the dithiol molecules to the electrodes[24] and found to be sensitive to the molecule bonding site.[25] So far, however, only very few experimental studies have been conducted on magnetic tunnel junctions and nickel break-junctions bridged by thiols[27] or dithiols,[28,29] and some of these

Received: May 6, 2015
Revised: June 9, 2015

DOI: 10.1021/acs.jpcc.5b04351
J. Phys. Chem. C XXXX, XXX, XXX−XXX

studies underlined the need for a deeper understanding of the growth of thiol SAMs on magnetic surfaces.[27] Indeed, it is clear that in order to assess, interpret, and control fundamental properties of these junctions at the experimental level, proper characterization and understanding of interfacial properties such as chemical bonding, hybridization, and molecular conformation at the molecule−metal junction are required. These interface-related properties not only determine the systems' stability but also drastically affect the spin injection at the organic−metal interface.[30,31]

Prompted by these considerations we have undertaken a comprehensive investigation of thiolate-bonded SAMs deposited on a Ni(111) single-crystal surface in UHV, whereby insight into the bonding, structure, and stability of the molecular monolayers has been gained by combining experimental spectroscopic tools for surface analysis and density functional theory (DFT) calculations. The Ni(111) surface has been selected due to the high surface quality and the ease of preparation in UHV, with the aim of performing a prototypical study in a well-defined and controllable environment. Moreover, the high Curie temperature of nickel (630 K) and the ability to grow epitaxial films of high crystalline quality in a (111)-orientation (for example, on a W(110) template[32,33]), which can be easily magnetized in UHV, render this surface an ideal playground for studying the coupling of organic molecules to ferromagnetic systems under model conditions via spin-dependent measurements.

Two precursor molecules have been selected for SAM formation: as illustrated in Figure 1, they both have a backbone

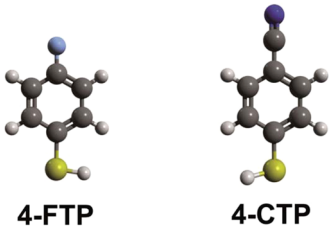

Figure 1. Molecular structure of 4-fluorothiophenol (4-FTP, left) and 4-cyanothiophenol (4-CTP, right), which were used here as precursor molecules for the formation of thiolate SAMs on Ni(111). Dark gray, C; light gray, H; yellow, S; light blue, F; violet, N.

that consists of a single phenyl ring attached to the thiol (SH) headgroup, whereas the end group is either a fluorine atom (4-fluorothiophenol, F−C_6H_4−SH) or a nitrile group (4-cyanothiophenol, NC−C_6H_4−SH). On gold[34−39] and copper[40−44] surfaces these molecules and the related compound thiophenol (C_6H_5−SH) are all known to form well-ordered SAMs, which are stable at room temperature (RT). Moreover, the charge delocalization across the aromatic backbone makes them good candidates for model studies of the ultrafast charge transfer across the molecule−metal interface.[38] In our combined experimental and theoretical study we focus on the competing factors that determine the adsorption geometry and the molecular packing in the monolayers. The coherent picture that emerges from the combined analysis allows us to rationalize the limited thermal stability of the SAMs and to address fundamental issues at the (sub)molecular level. In addition, changing the terminal functional group from fluorine to nitrile offers the opportunity to explore to what extent the end group affects the molecule-to-substrate coupling on Ni(111), compared to the relatively inert gold surfaces where the influence of the end group mainly results in a moderate change of the molecular tilt.[2,45]

The Article is organized as follows: the experimental procedures and computational details are described in sections 2.1 and 2.2, respectively. In section 3.1 we discuss the main experimental evidence for the formation of a well-defined SAM of 4-fluorothiophenol (4-FTP in the following) at 200 K, whereas section 3.2 deals with the temperature-dependent degradation of the SAM by mild annealing. The theoretical modeling of the 4-FTP adsorption on Ni(111), which provides in-depth insight into the structure and energetics of the SAM and offers a rationale for the thermally activated C−S bond scission, is discussed in section 3.3. Finally, the experimental evidence that additional end group−substrate interactions may profoundly affect the SAMs is presented in section 3.4, where the adsorption of 4-cyanothiophenol (4-CTP in the following) is examined. To conclude, the main achievements of the work are summarized in section 4.

2. EXPERIMENTAL AND COMPUTATIONAL DETAILS

2.1. Experimental Methods. The experiments were carried out in a custom-designed UHV chamber operating at a base pressure below 5×10^{-11} mbar, using radiation in the soft X-ray spectrum provided by the beamlines UE56/2-PGM-2 and U49/2-PGM-2 of the synchrotron radiation facility BESSY II in Berlin. Soft X-ray photoelectron spectroscopy (SXPS) data were recorded with a Phoibos 100 CCD hemispherical electron analyzer in a grazing incidence−normal emission geometry. The photon energy was chosen to be ∼100 eV above the respective core-level ionization threshold, to maximize both photoionization cross sections and surface sensitivity.[46] The Fermi edge measured under the same excitation and detection conditions as the respective core-level spectrum was used to calibrate the binding energy scale. To quantify the analysis of the photoelectron spectra, a Shirley-type background was subtracted, and a peak fitting routine based on Voigt functions was employed. Near edge X-ray absorption fine structure (NEXAFS) spectra were acquired using a homemade partial electron yield (PEY) detector that covers a large solid angle of $\sim\pi$ steradians and operates without high voltage.[47] To enhance the surface sensitivity of the PEY detection, retarding voltages were applied (−150 V at the C K-edge). Rotating the sample and the PEY analyzer simultaneously around the photon beam (incident at 7° with respect to the sample surface) resulted in a change of the direction of the **E** vector of the linearly polarized light relative to the sample surface without changing the detection geometry. The NEXAFS spectra were further processed by correction for the clean surface contribution to the absorption and for the incident photon flux according to standard procedures[48] and by subsequent normalization of the edge jump to one.

The same experimental chamber was also used off-line in our laboratories at the Technische Universität München, when equipped with a conventional dual anode X-ray source for nonmonochromatized Mg K_α and Al K_α radiation, and with a commercial VUV discharge lamp (Omicron HIS 13) fitted with a linear polarizer. Temperature-programmed desorption (TPD), ultraviolet photoelectron spectroscopy (UPS), and X-ray photoelectron spectroscopy (XPS) were used in these off-line experiments to further characterize the molecular layers, in particular to determine the desorption temperature of the multilayer, to monitor work function changes, and to assess the dependence of the valence band spectra on the light

DOI: 10.1021/acs.jpcc.5b04351
J. Phys. Chem. C XXXX, XXX, XXX−XXX

polarization direction. The UPS and XPS on-campus measurements were conducted using the He I line at 21.22 eV and the Al K_α line centered at 1486.6 eV (with ~0.8 eV broadening due to overlap of the $K_{\alpha1}$ and $K_{\alpha2}$ transitions), respectively.

The Ni(111) single-crystal surface was cleaned by repeated cycles of Ne^+ ion sputtering and annealing to 1100 K, until no contamination was detected by XPS and the low energy electron diffraction (LEED) pattern showed a sharp (1 × 1) structure. 4-FTP (liquid) was directly deposited onto the sample via a leak valve and a stainless steel dosing tube, whereas 4-CTP (solid) was sublimated by heating a quartz crucible loaded with molecular powder, which was moved in front of the sample surface. Unless otherwise stated, the substrate was held at 80 K when exposed to the molecular vapors.

Due to the different temperature at which desorption of condensed multilayers occurs for 4-FTP and 4-CTP, respectively, the protocol for SAM preparation differed between the two molecules. Multilayers of 4-FTP and 4-CTP molecules could be prepared under similar conditions, i.e., by depositing the respective molecules onto the nickel substrate kept at 80 K. TPD measurements on the 4-FTP multilayer at a heating rate of 2 K/s (see SI, Figure S1) yield a pronounced desorption peak for the intact molecule centered at ~190 K. A saturated monolayer of 4-FTP was therefore prepared from the multilayer by annealing the substrate to 200 K for a few seconds. Conversely, the desorption temperature of 4-CTP multilayers lies well above RT (340 K, Figure S1), and in order to preserve the integrity of the molecules in the first layer, a heating treatment above this temperature could not be performed. Instead, the monolayer was grown directly at 80 K, stopping the exposure of the substrate to the molecular beam after completion of the monolayer. This was checked by XPS, exploiting the distinct binding energy shift observed in the S 2p core level, due to the different chemical environment of molecules in the first and second layer (i.e., thiolates vs thiols). Subsequently, brief annealing to 200 K was performed to ensure conditions directly comparable to those of the 4-FTP SAMs.

During the synchrotron experiments at high photon brilliance the SAM-covered samples were routinely checked for beam damage, and precautions were taken to prevent such an effect, e.g., by scanning the photon beam over the sample area and by reducing the photon flux appropriately. Beam damage occurring at a rate significantly more rapid than the acquisition time of our measurements was not observed. In particular, XPS and NEXAFS measurements performed in low-alpha operation mode (beam current in the storage ring reduced by more than 1/10 relative to the normal hybrid-mode operation) gave entirely consistent results with measurements performed by scanning continuously the point of probing and did not show any progressive deterioration of the spectral fingerprints. Moreover, the X-ray electron spectroscopy measurements were typically performed at low temperature (80–100 K), as this is known to further reduce the effect of beam damage.[49,50]

2.2. Computational Methods. All calculations have been carried out with the VASP[51,52] and CASTEP[53] (Version 6.0.1) codes by solving the one-electron Kohn–Sham equation[54] within the generalized gradient approximation proposed by Perdew, Burke, and Ernzerhof (PBE)[55] to treat electronic exchange and correlation. Test calculations including dispersion-corrections (Tkatchenko and Scheffler scheme)[56] indicate only insignificant changes of the adsorption geometries and no qualitative changes in the calculated reaction energies. The one-electron Kohn–Sham orbitals were expanded in a plane wave basis set with an energy cutoff of 400 eV, and electron–ion interactions were described via standard-library potentials. The surface was represented by a five-layer slab, and in all calculations, we have allowed the relaxation of the substrate atoms in the two topmost metal layers (the substrate atoms in the three bottom layers were kept fixed in their bulk equilibrium positions), as well as all the atoms of the adsorbates. All the geometry optimizations were carried out until reaching forces on every mobile atom smaller than 0.02 eV/Å. The Brillouin zone sampling was carried out according to the Monkhorst and Pack method[57] with meshes (3 × 4 × 1), (5 × 5 × 1), (7 × 5 × 1), (7 × 5 × 1), and (7 × 7 × 1) for the unit cells (4 × 3), ($\sqrt{7} \times \sqrt{7}$), (2 × 3), ($\sqrt{3} \times \sqrt{7}$) ,and (2 × 2), respectively. All calculations are spin polarized.

We have determined reaction energies for the following reactions:

•Molecular adsorption

$$\varepsilon_1 = E_{F-C_6H_4-SH@Ni} - E_{Ni} - E_{F-C_6H_4-SH(gas)} \quad (1)$$

•S–H bond cleavage

$$\varepsilon_2 = E_{(F-C_6H_4-S+H)@Ni} - E_{Ni} - E_{F-C_6H_4-SH(gas)} \quad (2)$$

•H and F–C_6H_4–S phase separation

$$\varepsilon_3 = E_{F-C_6H_4-S@Ni} + E_{H@Ni} - 2E_{Ni} - E_{F-C_6H_4-SH(gas)} \quad (3)$$

•S–C bond cleavage + H adsorbed

$$\varepsilon_4 = E_{(F-C_6H_4+S)@Ni} + E_{H@Ni} - 2E_{Ni} - E_{F-C_6H_4-SH(gas)} \quad (4)$$

•H, F–C_6H_4, and S phase separation

$$\varepsilon_5 = E_{(F-C_6H_4)@Ni} + E_{H@Ni} + E_{S@Ni} - 3E_{Ni} - E_{F-C_6H_4-SH(gas)} \quad (5)$$

In eqs 1–5, $E_{X@Ni}$, E_{Ni}, and $E_{F-C6H4-SH(gas)}$ stand for the total energies of X adsorbed on Ni(111), the clean Ni(111) surface, and the F–C_6H_4–SH molecules in gas phase, respectively. $E_{(X+Y)@Ni}$ refers to the total energy of X and Y fragments simultaneously adsorbed within the same unit cell. A negative energy indicates a favorable process with respect to the initial state. For each molecular entity X (with X = F–C_6H_4–SH, F–C_6H_4–S, F–C_6H_4) adsorbed on the surface, we have explored different configurations with S (for F–C_6H_4–SH and F–C_6H_4–S) or C (for F–C_6H_4) initially located on high symmetry sites (top, bridge, fcc, and hcp), as well as different orientations of the phenyl ring. Initial geometries for X and Y (Y = H, S) coadsorption are created using the optimum geometry found for X adsorption and adding the Y coadsorbate within the same unit cell as far away as possible. Only hollow sites were considered for Y coadsorption, as calculations at coverage 0.08 ML showed that top and bridge sites are 1.5–1.6 eV (0.61–0.56 eV) and 0.2–0.3 eV (0.12–0.14 eV) less favorable than hollow sites for S (H) adsorption, respectively.

In order to propose a possible structural model for the thiolate (F–C_6H_4–S) SAM, we performed NEXAFS simulations for the C K-edge. Due to the strong dependence of adsorbed geometries with respect to the coverage, we also analyzed free-standing thiol overlayers (F–C_6H_4–SH) in addition to the coverages Θ = 0.14, 0.20, and 0.25 ML, for

DOI: 10.1021/acs.jpcc.5b04351
J. Phys. Chem. C XXXX, XXX, XXX–XXX

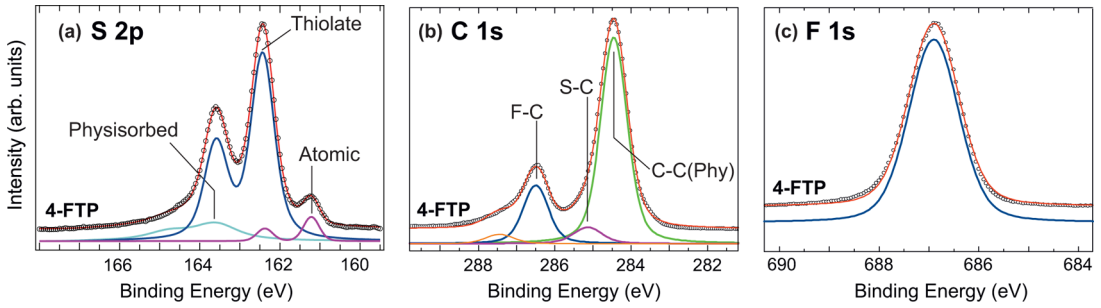

Figure 2. XP spectra (dots) and respective fitting (continuous lines, red) of a 4-FTP monolayer adsorbed on Ni(111): (a) S 2p; (b) C 1s; and (c) F 1s core-level regions. The results of the curve-fitting analysis are superimposed on the experimental data, with different colors corresponding to different components, whose attribution is discussed in the text. Note that the individual components have been downward-shifted relative to the experimental data for clarity. The S 2p, C 1s, and F 1s spectra were recorded at photon energy of 260 (a), 380 (b), and 800 eV (c), respectively.

which we performed the calculations including the Ni substrate. In those cases, we performed geometry optimizations for different molecular arrangements whose lateral spacing is imposed as would be imposed by the Ni surface. Once the optimum geometry at each coverage was obtained, we performed a NEXAFS analysis. The computation of the theoretical C 1s X-ray absorption spectra of the 4-FTP molecule in the different molecular adsorption geometries considers core to unoccupied orbital excitations as resulting from dipole transitions. To model the excited atom in which the hole is localized, a core−hole-excited pseudopotential was specially constructed and a PAW reconstruction approach was employed to correct the pseudopotential error in the matrix element evaluations. A full core hole was generated in the pseudopotential. Assuming perfect screening of the core−hole by metal electrons, the Fermi energy of the surface system was increased by one electron to yield charge-neutrality. For a full description of the CASTEP implementation of core-level spectroscopy the reader is referred to refs 58 and 59.

The computed spectra correspond to the following polarization-resolved intensities:

$$I(E,\theta) \approx \sum_k \omega_k \sum_n \gamma(E - E_{n,k})\left[\frac{1}{2}((M_x^{nk})^2 + (M_y^{nk})^2)\sin^2(\theta) + (M_z^{nk})^2\cos^2(\theta)\right] \quad (6)$$

where θ is the angle between the polarization vector of the incoming radiation and the surface normal, M_α^{nk} with $\alpha = x, y, z$ is the dipole transition matrix element involving the initial core state ψ_c and a final unoccupied state ψ_{nk}, and $\gamma(E - E_{n,k})$ is a Gaussian broadening function used in the Brillouin zone spectral integration. Equation 6 has been obtained taking into account the hexagonal symmetry of the surface.[60] Numerical convergence of the spectra with respect to both energy cutoff and k-point density has been carefully tested. For each geometrical configuration, the average C K-edge spectra were analyzed. Although the chemical shift for each carbon atom would in principle be different, we have checked that the dichroism for each atom is the same.

3. RESULTS AND DISCUSSION

In this section we focus on the characterization of the *in situ* prepared SAMs consisting of a single organic layer on top of the Ni(111) surface. In the 4-FTP case, well-defined SAMs could be prepared at 200 K, and therefore, detailed DFT calculations were performed in order to shed light on the adsorption structure and bonding. In the 4-CTP case, the situation is more complex, with partial fragmentation possibly occurring. Although a thorough DFT analysis could not be attempted, it is possible to draw conclusions about the importance of the terminal group.

3.1. SAM of 4-Fluorothiophenol on Ni(111). Figure 2 shows representative XP spectra of the S 2p, C 1s, and F 1s core levels for a 4-FTP monolayer prepared as described in section 2.1. The high-resolution XPS data convey information on the elemental composition, chemical environment, and integrity of the molecular overlayer. The S 2p spectrum (Figure 2a) is dominated by a spin−orbit split doublet (blue curve) with the S $2p_{3/2}$ component located at a binding energy of 162.4 eV. This value is typical for thiolate bonding to the Ni(111) surface and thus indicates the anchoring of the molecules to the substrate through the thiol headgroup.[61−63] The thiolate bond is established upon cleavage of the S−H bond followed by formation of the metal−sulfur bond. Further evidence for the thiolate formation is given by the comparison with a condensed multilayer of intact 4-FTP molecules (SI, Figure S2), where the S 2p doublet is shifted to significantly higher binding energy, the S $2p_{3/2}$ component of the intact S−H group being centered at 163.5 eV.[62] The analysis of the fitted intensities presented in Figure 2a indicates that ∼80% of the molecules in the 4-FTP monolayer are in this particular chemical state with the deprotonated thiol group. The much weaker spectral feature at the lower binding energy of 161.2 eV is often assigned to atomic sulfur on the nickel surface,[62,64,65] which results from S−C bond scission, and we also come to a similar conclusion. Under some circumstances this process can be competing with the formation of thiolate bonds and is strongly dependent on the temperature, as will be further detailed below. After brief annealing to 200 K, however, the relative amount of atomic sulfur is only ∼5% for 4-FTP and can therefore be neglected in the following discussion. It is worth noting that even for thiolate-bonded SAMs on gold a component that can be attributed to atomic sulfur has been occasionally observed,[39,66−68] although a different interpretation for its origin has been tentatively proposed.[69] In the present case, dissociation of the molecule possibly occurs at step edges and defects of the nickel single-crystal surface and is increasingly hindered at low temperatures, as indicated by experiments on SAMs deposited at 80 K (not shown) where the low binding energy component is quenched. Besides, an additional (broader) doublet feature can be identified at higher binding energy (S $2p_{3/2}$ at 163.6 eV), which is most likely due to differently bound species or byproducts, either disulfide

DOI: 10.1021/acs.jpcc.5b04351
J. Phys. Chem. C XXXX, XXX, XXX−XXX

species[70] or physisorbed (unbound) molecules that remain trapped following desorption of the multilayer.[39,70,71]

As for the C 1s XP spectrum, the 4-FTP monolayer displays an intense line located at a binding energy of 284.5 eV (plotted in green in the curve-fitting analysis of Figure 2b). This signal can be attributed to photoemission from the carbon atoms of the phenyl ring, which are bonded to hydrogen, whereas the component at higher binding energy (286.5 eV, blue curve) originates from the carbon atom bonded to the highly electronegative fluorine substituent. A component at intermediate binding energy (285.1 eV, pink curve) is also visible in the fitted spectrum and can be ascribed to the carbon atom attached to the thiol group, in line with the interpretation of related X-ray absorption studies.[35,44] Finally, an additional component at about 287.5 eV, which appears as a weak high-energy shoulder in Figure 2b (orange curve), is necessary to obtain an acceptable fit but could not be unambiguously assigned. It possibly stems from shakeup processes or, alternatively, from minority species on the surface.

Core-level photoemission from the terminal atom at the end group provides further information on the integrity of the SAM molecules upon adsorption and on their interaction with the nickel substrate. Indeed, the F 1s core-level intensity shows a single component located at 686.9 eV. This value is only marginally different from that found for 4-FTP multilayers (686.95 eV; Figure S2 in the SI), thus indicating that the F atom does not undergo a distinct change of chemical environment and is most likely tilted away from the surface and not directly involved in the interaction with the metal substrate. Notably, the binding energy of atomic fluorine adsorbed onto the Ni(111) surface lies significantly lower (683.8 eV[72]), and therefore, taken together, the XPS results give conclusive evidence of the integrity of the 4-FTP SAMs at 200 K.

The picture of the molecule−metal interaction that emerges from the XPS data is corroborated by the angle-dependent NEXAFS measurements reported in Figure 3, which elucidate the adsorption geometry of the molecules in a direct way. The C K-edge spectra of the 4-FTP monolayer exhibit a strong dependence on the polarization of the incident radiation. Of the two clearly distinguishable resonances appearing below the continuum step, the first (dominant) one centered at 285.2 eV is assigned to the resonant excitation of an electron from the C 1s level of the aromatic carbon backbone (specifically, the four carbon atoms bonded to H) into the lowest unoccupied molecular orbital (LUMO) of π^* character and the second at 287.4 eV to the analogous transition from the fluorinated carbon of the phenyl ring. A third spectral feature is associated with the transition from the C 1s level of the S-bonded C atom into the LUMO and results in a weaker shoulder on the right side of the main resonance (~285.8 eV). This assignment, supported by the comparison with the multilayer spectra (SI, Figure S3), is in agreement with previous literature.[35,44] The fact that the π^* resonances display maximum intensity at θ = 90°, when the electric field of the radiation is parallel to the surface, clearly demonstrates an upright orientation of the molecular plane in the monolayer. However, a non-negligible tilt from the surface normal can be inferred since the resonances are not completely quenched at θ = 7°, a geometry in which the electric field is directed almost perpendicular to the surface. Quantitative analysis based on curve fitting at three angles of the polarization relative to the surface normal (7°, 50°, and 90°) yields a value of 30° for such a tilt, corresponding to an average adsorption angle of α_{exp} = 60° ± 10° as depicted schematically in the inset of Figure 3.

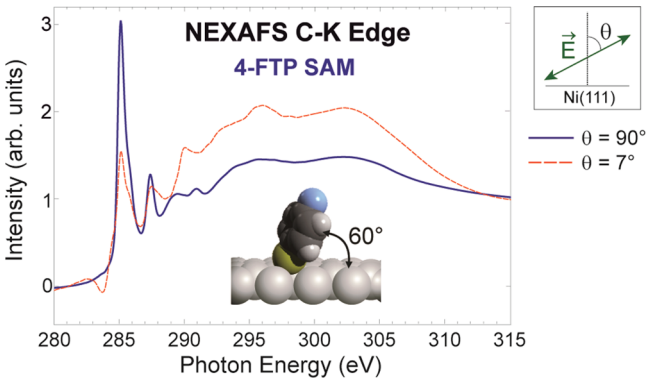

Figure 3. NEXAFS spectra at the carbon K-edge of a 4-FTP monolayer for two different geometries corresponding to electric field of the radiation parallel (θ = 90°) or almost perpendicular (θ = 7°) to the surface. The estimated adsorption angle of the molecular plane is shown in a pictorial fashion in the inset.

Finally, we determined the work function of the 4-FTP SAMs by means of UPS, with the sample negatively biased at −5 V to increase the kinetic energy of the escaping electrons and measure precisely the secondary electron cutoff. We found that the adsorbed monolayer causes a lowering of the work function with respect to the bare Ni(111) surface by $\Delta\varphi_{exp}$ = −0.6 ± 0.1 eV. Interestingly, in the SAM grown on Cu(100) the same molecule was found to induce a considerably smaller change and of opposite sign, $\Delta\varphi$ = +0.16 eV, in spite of the very similar molecular orientation (adsorption angle of 65°).[44]

3.2. Thermal Stability of the 4-Fluorothiophenol SAM.

The experimental results presented in section 3.1 demonstrate that a well-defined thiolate-bonded 4-FTP monolayer can be prepared at 200 K. However, in view of technological applications an important issue concerns the thermal stability of this SAM. It is well-known, for example, that thiolate SAMs are stable on gold surfaces at 300 K (ref 2) and that the upper limit for the stability is located somewhere around 400 K,[73−76] being mainly dictated by the stability of the Au−S bond. In the case of the more reactive Ni(111) surface, a much different behavior is expected. While the cleavage of the S−H on Ni(111) already occurs at the lowest temperature used in this work (80 K), the stability of the resulting thiolate bonding at the molecule−metal interface is limited primarily by the occurrence of C−S bond breaking, which leaves atomic sulfur on the surface and, possibly, coadsorbed molecular fragments. Figure 4 presents relevant core-level spectra recorded after sequential annealing of a 4-FTP multilayer to increasing temperatures. To reach the final temperature in each annealing step a constant heating rate of 2 K/s was used. The curves recorded after annealing to 200 K correspond to the intact thiolate SAM described above. However, upon heating to 250 K it is evident from inspection of panel (a) that the proportion of atomic sulfur increases dramatically and that an admixture of thiolate and chemisorbed atomic sulfur covers the surface. The C−S bond cleavage proceeds further at 300 K, such that atomic sulfur by far dominates in the overlayer composition at this temperature.

In parallel with the change of the S 2p spectrum, the C 1s and F 1s spectra display a distinct evolution, where the progressive decrease of both elemental species denotes partial

DOI: 10.1021/acs.jpcc.5b04351
J. Phys. Chem. C XXXX, XXX, XXX−XXX

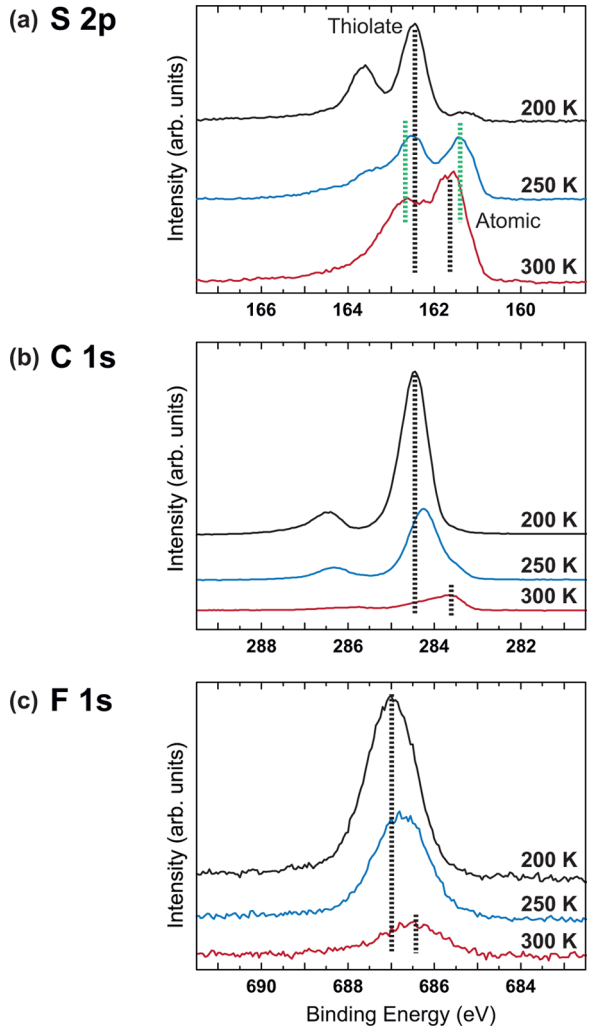

Figure 4. XP core-level spectra of the saturated 4-FTP SAM acquired after heating the surface to increasing temperature with 2 K/s heating rate. (a) In the S 2p spectrum, the thiolate and atomic S components are marked by vertical dotted lines (black and green lines highlighting small binding energy shifts). The formation of atomic sulfur at temperatures above 200 K is clearly visible and demonstrates unambiguously that the monolayer is not stable at RT. The (b) C 1s and (c) F 1s spectra also display a distinct evolution attributable to deterioration of the layer and molecular decomposition. Binding energy shifts at different temperatures are highlighted by dashed lines (see also text). The photon energy used for each core level is the same as that in Figure 2. After annealing, all spectra were measured at low temperature (80 K).

desorption of the fragments formed upon molecular decomposition. These fragments contain, primarily, the aromatic ring in closer proximity to the surface, as indicated by a distinct shift to lower binding energy (this probably arises from a combination of true chemical shift and enhanced screening of the core hole in the final state created by photoemission); however, at 300 K atomic carbon may also be present. Note that in the 300 K data the binding energy of the F 1s core level is lowered to 686.4 eV, with a shift of −0.6 eV compared to the intact monolayer. This binding energy value is not compatible with the presence of coadsorbed atomic F,[72] and it rather suggests that the fluorine left in the layer remains mostly bound to the phenyl ring, albeit lying closer to the metal surface.

We should also mention that increasing the temperature above 250 K might eventually drive restructuring of the Ni(111) surface, as observed for methanethiolate (CH_3S-) and coadsorbed atomic S on the same surface.[63,77,78] Although small but detectable binding energy shifts to higher binding energy at increasing temperature (marked by the green and black vertical lines in Figure 4a) are consistent with this phenomenon, we refrain from definitive conclusions based solely on the XPS data.

The obvious implication is that the 4-FTP SAM exhibits only limited stability and, unlike on gold, it is not intact at room temperature. C−S bond scission is thermally activated above 200 K, and considering the stability of 4-FTP in the liquid phase at 300 K, this indicates that the strong S−Ni interaction does weaken the headgroup-to-backbone bond in the molecules, leading to facile C−S bond breaking. These results are in excellent agreement with a previous study of adsorbed thiophenol (benzenethiol) on Ni(111),[62] where S−C bond scission was found to be the preferred pathway above 190 K. Conversely, methanethiolate starts to dissociate on Ni(111) at even lower temperatures (150 K),[65] although the onset of the C−S bond scission was shown to shift above 200 K at increasing molecular coverage.[63,65] Finally, for cyclohexanethiol on Ni(111) the activation of the C−S bond was shown to start in the 180−240 K temperature range with an earlier onset at low coverage.[79]

In striking contrast to these findings, a number of more recent works conducted on thiol SAMs deposited by wet-chemical methods on plain and textured polycrystalline Ni films claim that formation of pure thiolate-bonded monolayers (without detectable amount of atomic sulfur) can be achieved at RT.[14,15,19,80−83] It is certainly possible that the higher stability is related to the different preparation method employed and, possibly, to the higher packing density that can be obtained in the SAMs via deposition from solution.[2] Moreover, the wet-chemically prepared SAMs were mostly deposited onto polycrystalline nickel (where the surface structure and possible restructuring effects may play a different role) and were based on alkanethiols of varying length (which might exhibit increased stability of the C−S bond in the adsorbed layer as compared with aromatic thiols); this could be at the root of the discrepancies observed with respect to the vapor-phase experiments. In addition, in all cases but one[83] some detectable amount of oxygen was found on the polycrystalline nickel substrates, owing to the methods employed for surface preparation and cleaning outside the UHV environment. Nonetheless, to cast light on the stability issue we have investigated the effect of the substrate temperature further, specifically by directly depositing the SAM onto the Ni(111) substrate held at 300 K. To this purpose, the Ni(111) surface was exposed to the same amount of 4-FTP molecules used to condense a multilayer at 80 K. Figure 5 shows the corresponding S 2p XP spectrum, along with the respective curve-fitting analysis. Clearly, the spectrum is indicative of an ill-defined monolayer containing a significant proportion of atomic sulfur, in excess to 35% of the total S amount. This confirms that RT-stable, well-defined 4-FTP SAMs consisting of only intact thiolate moieties cannot be attained by adsorption from the vapor phase.

We note that the global line-shape of the S 2p core level of Figure 5, which results from the overlap of at least two distinct spin−orbit split doublets, closely resembles that of a single spin−orbit doublet recorded at low instrumental resolution.

DOI: 10.1021/acs.jpcc.5b04351
J. Phys. Chem. C XXXX, XXX, XXX−XXX

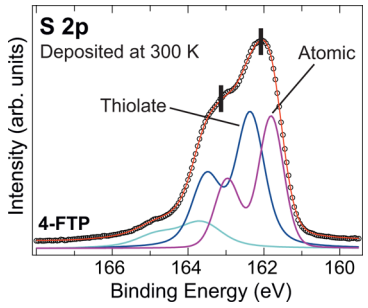

Figure 5. S 2p XP spectrum (photon energy: 260 eV) from a 4-FTP monolayer deposited onto the Ni substrate held at 300 K. Black dots correspond to the experimental data, while the solid lines display curve-fitting results (with spin−orbit split doublets marked by the same color). The individual components of the fit are vertically shifted relative to the experimental data for clarity. The film is ill-defined and contains a considerable amount of atomic sulfur, as shown by the curve-fitting analysis.

Indeed, the separation between the main maximum at 162.1 eV and the shoulder at ∼163.2 eV (marked by black bars in Figure 5) is very close to the spin−orbit splitting (1.1−1.2 eV) of the S 2p core-level.[84,85] It is the detailed curve-fitting analysis combined with the high counting rate and the high energy resolution achievable with synchrotron radiation (see also the sharp photoemission lines in Figure 2a) that allows us to disentangle the individual contributions to the broadened line-shape. Nonetheless, even at the highest resolution of our measurements (∼0.1 eV) it is arduous to get a unique fit for the RT S 2p spectrum due to the broadened line-shape: the fitting shown in Figure 5 has been performed constraining the thiolate component to the same binding energy of the 200 K spectrum (162.4 eV), while letting it free still leads to good fits but with a considerably higher proportion of atomic S. However, the S 2p XP spectra used in previous works on solution-prepared SAMs to reaffirm the integrity of the thiolate bond are usually taken at lower resolution (>0.4 eV), yielding broadened S 2p line-shapes very similar to that of Figure 5 in both width and position (in some cases the center-of-gravity is slightly shifted to lower binding energy).[14,15,19,80−83] Therefore, it is likely that even those samples that (without relying on quantitative curve-fitting analysis) are claimed to have 100% of thiolate species in fact contain a non-negligible amount of atomic sulfur.

Our findings not only prove the limited stability of the thiolate SAMs deposited from vapor phase but also strongly emphasize the need for high-resolution data in order to resolve this long-standing controversy for differently prepared systems and the importance of studying the effect of coadsorbed atomic species (e.g., atomic oxygen) on the C−S bond activation.

3.3. DFT Calculations of Adsorbed 4-Fluorothiophenol on Ni(111). To gain more insight into the 4-FTP-Ni bonding and to rationalize the structural details of the FTP-SAM, we have performed DFT calculations focusing on the energetics and local adsorption geometry at different molecular coverages.

3.3.1. Energetics. Figure 6 details the full energy profile for F−C_6H_4−SH adsorption on Ni(111) at representative coverages, specifically Θ = 0.14, 0.20, and 0.25 ML. In this picture, reaction energies ε_1 to ε_5 correspond to the processes listed in eqs 1−5. At coverage Θ = 0.08 ML, both molecular adsorption (ε_1 = −0.70 eV) and H−S bond cleavage (ε_2 = −2.33 eV) are highly exothermic reactions. Calculations of H_2 associative desorption indicate that this reaction step is endothermic by 1.36 eV. As a result, after H−S bond cleavage both H and thiolate should be present on the surface. However, H and thiolate are very mobile on the surface[86] favoring phase separation (i.e., thiolate and H will arrange on different regions of the surface). Note that the mobility of these species, including thiol, is essential to continue the reaction process as the coverage increases. At coverage Θ = 0.14 ML (Figure 6, red lines), all the reaction steps are still downhill in terms of energy. Molecular adsorption (ε_1 = −0.62 eV) and H−S (ε_2 = −1.76 eV) and S−C (ε_4 = −2.05 eV) bond cleavages are all highly exothermic reactions producing H, F−C_6H_4, and S fragments adsorbed on the surface.

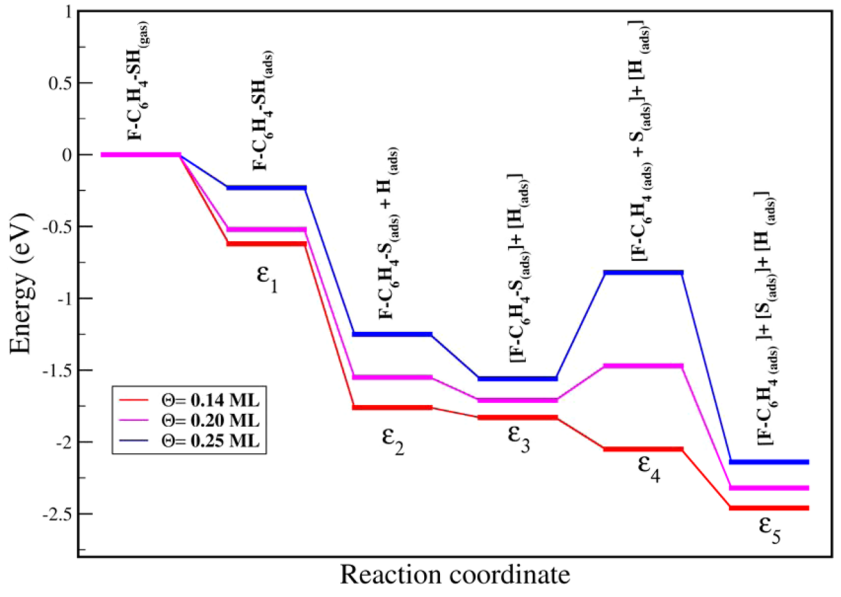

Figure 6. Calculated energy profile for coverages Θ = 0.14, 0.20, and 0.25 ML. Reaction energies ε_1−ε_5 correspond to the processes described in eqs 1−5; see text.

DOI: 10.1021/acs.jpcc.5b04351
J. Phys. Chem. C XXXX, XXX, XXX−XXX

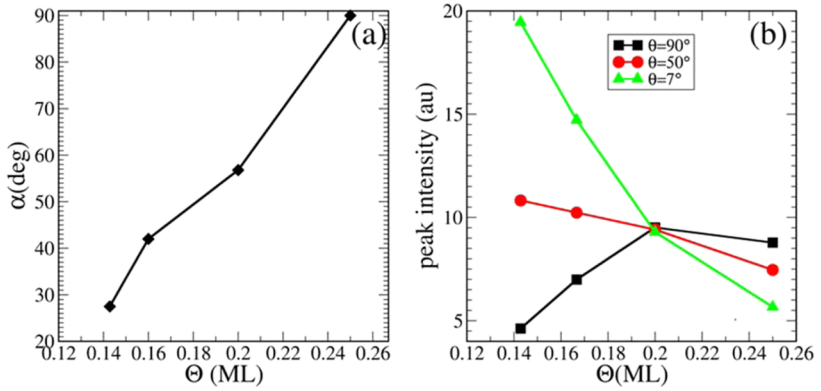

Figure 7. Calculations for a free-standing thiol SAM. (a) Tilt angle α as a function of coverage. (b) Peak height corresponding to the leading peak of the NEXAFS C K-edge for different angles θ of the photon polarization vector relative to the surface normal; see text.

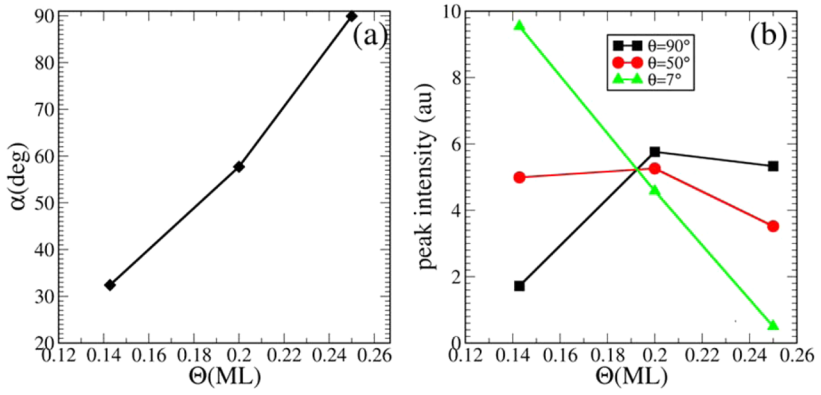

Figure 8. Calculations for a thiolate SAM on Ni(111). (a) Tilt angle α as a function of coverage. (b) Peak height corresponding to the leading peak of the NEXAFS C K-edge for different angles θ of the photon polarization vector relative to the surface normal; see text.

At coverage Θ = 0.20 ML (Figure 6, pink lines), this situation starts to change. The energy profile is still downhill before reaction step 4. Molecular adsorption (ε_1 = −0.52 eV) and H−S bond cleavage (ε_2 = −1.55 eV) are thus favored thermodynamically. However, S−C bond scission now becomes endothermic (the energy difference between reaction steps 3 and 4 is +0.24 eV). This development continues at coverage Θ = 0.25 ML (Figure 6, blue lines), where the energy profile is downhill until reaction step 4 as before. Molecular adsorption (with ε_1 = −0.23 eV) and H−S bond cleavage (ε_2 = −1.25 eV) are thus still favored thermodynamically. However, S−C bond scission becomes even more endothermic (the energy difference between reaction steps 3 and 4 is now +0.74 eV), suggesting that the thiolate coverage is getting too high.

Comparing to the experimental finding of limited thermal stability of the thiolate SAM (S−C bond scission thermally activated above 200 K), these calculated energy profiles suggest the experimental coverage to lie around and above 0.2 ML (where S−C bond scission becomes energetically activated).

We note, however, that our experimental layer preparation starts from Θ = 0, including for a short time the coverage regime where S−C dissociation is not activated and exothermic bond breaking followed by fragment adsorption should become possible even at low temperature. Because of the negligible amount of atomic S seen in XPS for adsorption at 80 K, this reaction must be slow. This could be due to a low pre-exponential because of steric hindrance; however, a clarification is not possible without future theoretical work including entropic effects. Moreover, from the experimental point of view, we cannot make conclusions on the growth mechanism, which could involve island formation (i.e., higher local coverage) in the early stages of growth: dedicated scanning tunneling microscopy (STM) experiments could be interesting in attempting to clarify this issue.

3.3.2. Geometry. Concerning the predicted adsorption geometries of adsorbed fragments, we observe a complex coverage dependence. As expected, the phenyl ring tends to adopt a more upright configuration as the coverage increases. In addition, for some species the predicted adsorption sites also change with coverage. In the case of thiols, for instance, (i) the tilt angle of the phenyl ring with respect to the surface plane (α) increases from α = 49° at Θ = 0.08 ML to α = 90° at Θ = 0.25 ML and (ii) the S atom always lies close to bridge sites at 1.83−1.86 Å from the surface. For thiolate species (i) α was calculated to go from 5° at Θ = 0.08 ML to α = 90° at Θ = 0.25 ML (at the intermediate coverage Θ = 0.14 ML, α = 34°), and (ii) S lies close to bridge, bridge-hcp, and fcc sites at Θ = 0.08, 0.14, and 0.25 ML, respectively (the height of S above the surface decreases from 1.85 to 1.60 Å as the coverage increases).

The experimental results indicate that below 200 K (i) the monolayer is mainly formed by thiolate (∼80% of molecules in the monolayer are in this particular state, according to XPS) and (ii) the tilt angle of the phenyl ring with respect to the surface plane is α_{exp} = 60° ± 10°. Therefore, our theoretical calculations suggest that the experimental structure can be rationalized with a coverage between 0.14 and 0.25 ML.

DOI: 10.1021/acs.jpcc.5b04351
J. Phys. Chem. C XXXX, XXX, XXX−XXX

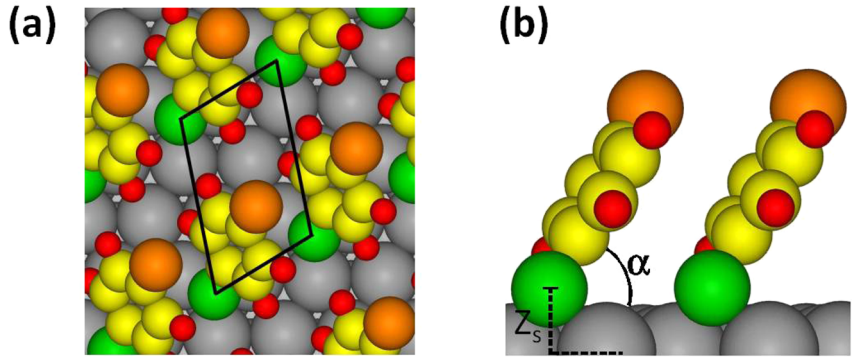

Figure 9. (a) Top and (b) side views of 4-FTP thiolate at the preferred adsorption geometry for a coverage Θ = 0.2 ML. Additionally shown in panel (b) are definitions of the geometry parameters Z_S and α (see text).

3.3.3. NEXAFS. In order to specify this further, we proceed to simulate the dichroism of the leading NEXAFS signature. This provides a unique opportunity to indirectly extract the coverage from the NEXAFS dichroism. In order to get insight into this issue we first consider a simple model based on a free-standing thiol SAM (without the presence of a metal slab). As a second step, we tackle the real thiolate-SAM/Ni(111) system.

Figure 7 shows the results obtained for free-standing thiol monolayers in the coverage range 0.14 ML ≤ Θ ≤ 0.25 ML (we define the coverage as it would be defined if the Ni(111) surface was included). As expected, the tilt angle α of the thiol molecule increases with increasing coverage (Figure 7a). In Figure 7b, we plot the height of the leading peak observed in the simulated C K-edge NEXAFS spectra for different angles of the polarization vector θ (θ = 7°, 50°, 90°) as a function of the coverage. This demonstrates clearly that the predicted C K-edge dichroism is sensitive to coverage. From these calculations one can therefore deduce that the experimental coverage should exceed ∼0.2 ML in order to obtain the right dichroism (at the leading peak the maximum intensity must be obtained for θ = 90°). This is not perfectly quantitative, however, since (i) our calculations do not include the substrate and (ii) coverage/exposure-dependent NEXAFS experiments were not rigorously pursued.

Figure 8 shows the results obtained for the real thiolate-SAM/Ni(111) system. Due to the limitations in computationally tractable supercell size, these calculations are restricted to coverages Θ = 0.14, 0.2, and 0.25 ML. Comparing the data with and without explicit inclusion of the Ni(111) surface, Figures 7b and 8b, we observe only a modest effect of the substrate on the tilt angle of the overlayer. Similarly to the NEXAFS results obtained for the free-standing overlayer, the calculations explicitly including the surface thus confirm that the correct dichroism of the C K-edge is obtained for coverages Θ ≥ 0.2 ML. Moreover, to reproduce the experimentally determined molecular orientation, Θ = 0.25 ML has to be considered as an upper boundary.[87]

3.3.4. Theoretical Conclusion. Combining the information obtained from the calculated energetics, geometry, and NEXAFS spectra, we arrive conclusively at an estimate of the experimental coverage of 0.2 ≥ Θ > 0.25 ML. In this coverage range the correct dichroism for the C K-edge is obtained, while the energetics predict an endothermic reaction for the scission of the C−S bond. At coverages above 0.25 ML, it is predicted that the tilt angle will be larger than that found experimentally, whereas at 0.2 ML the tilt angle of the aromatic moiety relative to the sample surface is α = 58°, in excellent agreement with the experimental determination of α_{exp} = 60° ± 10°. In this geometry, the S headgroup lies close to a bridge-hollow (almost on hollow) site at Z_S =1.66 Å above the top surface layer (see Figure 9), and the rumpling in the first metal layer is Δ_z = 0.07 Å. Our calculations also reveal that the work function change of Ni(111) induced by thiolate adsorption is $\Delta\varphi_{theo}$ = −0.49 eV at this coverage, which is again perfectly consistent with the experimental one, $\Delta\varphi_{exp}$ = −0.6 ± 0.1 eV. All these results together thus indicate that the molecular arrangement found for Θ = 0.2 ML is a plausible model to explain the experimental SAM's structure.

It is worthwhile to note that the similarities obtained for free-standing and supported layers show clearly that the tilt angle of thiolate radicals (and therewith the indirect coverage determination) is dictated by the packing in the molecular layer, not by the local anchoring to a specific site on the surface.

3.4. SAM of 4-Cyanothiophenol on Ni(111). An experimental investigation, analogous to the 4-FTP counterpart and based on high-resolution XPS and NEXAFS, was conducted on a 4-CTP SAM prepared by incremental deposition of molecules up to a complete monolayer, followed by brief annealing at 200 K.

The S 2p core-level spectrum (Figure 10a) is very similar to that of the 4-FTP molecule (Figure 2a), and there is a distinct chemical shift of 1.5 eV to lower binding energy when moving from the multilayer to the 200 K annealed monolayer (SI, Figure S4). In the latter, a binding energy of 162.25 eV is found for the S $2p_{3/2}$ component, which indicates the formation of a thiolate-bonded monolayer. The relative amount of atomic sulfur (about 5%) is again much smaller than the proportion of dominant thiolate species (80% in this case), whereas a minority of physisorbed or unbound molecules also remain trapped in the monolayer. Moreover, similarly to the 4-FTP case, C−S bond breaking occurs upon annealing above 200 K (data not shown).

Despite these similarities, notable differences with respect to the 4-FTP SAMs emerge when inspecting the C 1s core-level region (Figure 10b). Here, the signal originating from the carbon atoms of the aromatic backbone (peak at 284.4 eV, green curve in Figure 10b) dominates, but the contribution associated with the S-bonded carbon of the phenyl ring (pink, 284.9 eV) is clearly discernible, giving rise to a shoulder on the high binding energy side of the main peak. Moreover, two additional components appear at a binding energy of 285.4 eV (violet) and 283.9 eV (black), respectively. The former spectral feature is associated with emission from the nitrile carbon[39,88] and is considerably weaker than the S−C ascribed C 1s signal,

DOI: 10.1021/acs.jpcc.5b04351
J. Phys. Chem. C XXXX, XXX, XXX−XXX

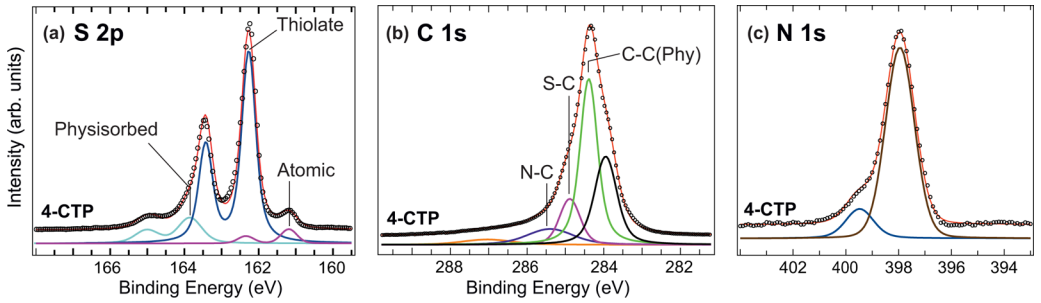

Figure 10. XP spectra (dots) and respective fitting (continuous lines, red) of a 4-CTP monolayer adsorbed on Ni(111): (a) S 2p; (b) C 1s; and (c) N 1s core-level regions. The results of the curve-fitting analysis are superimposed on the experimental data, with different colors corresponding to different components, whose attribution is discussed in the text. The individual components of the fit are vertically shifted relative to the experimental data for clarity. The S 2p, C 1s, and N 1s spectra were recorded at photon energy of 260 (a), 380 (b), and 500 eV (c), respectively.

while the latter cannot be straightforwardly attributed to any species of the intact molecule and will be considered in more detail below. As in the case of the 4-FTP SAMs, a rather weak component of unclear origin is placed by the fitting analysis close to 287 eV (orange curve).

Comparing the curve-fitted C 1s spectra of 4-FTP and 4-CTP monolayers, a clear difference in the relative photoemission intensity of the S-bonded carbon atoms (pink curves in Figures 2b and 10b) is observed. Specifically, the more pronounced C−S signal in the 4-CTP SAM can be explained by the lower degree of attenuation experienced by the outgoing photoelectrons due to scattering within the 4-CTP overlayer. This suggests a flatter configuration of the chemisorbed 4-CTP molecules compared to 4-FTP, as will be justified more convincingly by NEXAFS. Note that for 4-CTP it cannot be ruled out that some photoelectron signal from the carbon atoms bonded to the nitrile group (C−CN) falls close to the C−S derived signal;[88,89] however, the evidence discussed below indicates that this is a secondary contribution as the breaking of the C−CN bond tends to predominantly occur.

The N 1s core-level spectrum presented in Figure 10c exhibits a major peak at a binding energy of 397.9 eV, a value ∼1.1 eV lower than that in the condensed multilayer (Figure S4). This piece of evidence points to a pronounced interaction of the nitrile end group with the nickel substrate, which significantly perturbs the electronic environment of the N atoms in the monolayer and, in agreement with the previous argument, is consistent with predominantly lying-down adsorption of the molecules.[90] Conversely, the minority species at about 399.5 eV can be related to intact CN end groups more distant from the surface, either in molecules with a standing-up configuration and/or in the unbound species discussed above. This interpretation is corroborated by previous investigations on the adsorption of benzonitrile (C_6H_5−CN) on nickel and palladium surfaces,[89,91] and it leads us to conclude that the vast majority of the 4-CTP molecules anchored to the Ni(111) substrate through the thiolate group show a considerable interaction of their end group with the metal atoms at the surface. A pertinent question is therefore whether such an interaction still preserves the integrity of the molecule, merely leading to an opening of the C ≡ N triple bond by rehybridization of the C and N orbitals with the metal, or it instead results in partial dissociation of the 4-CTP molecules. In this regard, one needs to draw attention to the low binding energy component at 283.9 eV in the XP C 1s spectrum (black curve, Figure 10b). Such a component is completely absent in the multilayer spectrum (Figure S4) and can most likely be related to cleavage of the C−CN bond leading to atomic carbon on the surface and/or CN fragments with weakened triple bonds.[92] Notably, this component is significantly more intense than the (broader) high energy component at 285.4 eV associated with the nitrile carbon[39,88] of the intact molecules. In the multilayer the latter is chemically shifted by ∼1.5 eV relative to the phenyl ring derived component and leads to a pronounced shoulder (Figure S4, central panel) at the trailing edge of the C 1s line, whereas it is barely observable in the monolayer without fitting analysis. Therefore, we conclude that a large fraction of the 4-CTP molecules undergo dissociation upon adsorption.

Based solely on the XPS data, it cannot be established unambiguously whether the CN fragments formed by molecular dissociation remain anchored to the surface or further decompose into adsorbed atomic C and N. However, the C 1s and N 1s binding energies of 283.9 and 397.9 eV fall close to, but not exactly inside, the range of those reported for atomic C and N species adsorbed on nickel surfaces,[93,94] being higher by some 0.5 eV or more. This suggests that CN residues are still present, at least to some extent, on the surface at 200 K. This appears plausible, in view of the fact that, on Ni(111), hydrogen cyanide and the dehydrogenated CN fragments are known to dissociate into their atomic constituents at considerably higher temperatures,[95,96] and that, on the same surface, the decomposition of benzonitrile has been shown to proceed preferentially via scission of the C−CN bond rather than by further breakage of the stronger CN bond.[97]

Further evidence for the distinct molecule−substrate interaction in the 4-CTP SAMs compared to the 4-FTP counterpart is provided by NEXAFS. Indeed, the intensity contrast (linear dichroism) of the angle-dependent C K-edge absorption spectra of Figure 11 is reversed with respect to the 4-FTP case (Figure 3). The weak intensity of the π^* resonances at $\theta = 90°$ now indicates that the majority of the molecules lies with the phenyl ring much more tilted toward the surface (the average adsorption angle can be roughly estimated ∼30°−35°, but one should note that the contribution of the minority species mentioned above cannot be disentangled). This adsorption configuration facilitates the interaction of the CN end group with the surface and may be driving the decomposition of the molecules. An important implication is that, due to the different orientation, the molecular coverage for the full monolayer of 4-CTP is considerably lower than for the saturated monolayer of 4-FTP, as also confirmed by XPS (SI, Figure S5). Moreover, we should note that the (expected)[38] characteristic NEXAFS fingerprint obtained at the N K-edge of

DOI: 10.1021/acs.jpcc.5b04351
J. Phys. Chem. C XXXX, XXX, XXX−XXX

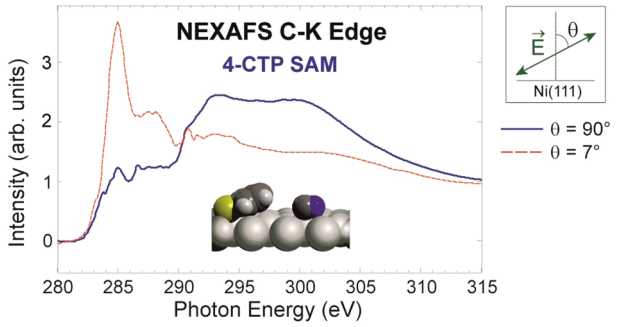

Figure 11. NEXAFS spectra at the C K-edge of a 4-CTP monolayer for two different light polarization geometries corresponding to electric field of the radiation parallel (θ = 90°) or almost normal (θ = 7°) to the surface. The adsorption configuration and the C−CN bond cleavage discussed in the text are sketched pictorially in the right panel.

the 4-CTP multilayer (SI, Figure S6) allows us to rule out the possibility that in our experiments the 4-CTP molecules decompose upon sublimation of the organic powder. This further emphasizes the importance of the end group for the adsorption.

Finally, we have conducted a set of experiments to exclude any effect of the different preparation method utilized for growing the 4-CTP and 4-FTP SAMs on the distinct pattern of the molecule−metal interaction. To this end, we prepared the 4-FTP SAM under conditions similar to those adopted for the 4-CTP SAM, by adding incremental doses of 4-FTP up to completion of the first layer, with low deposition rates and final annealing step at 200 K. The results of XPS and polarization-dependent UPS measurements reported in the Supporting Information (Figures S7 and S8) show unambiguously that the electronic and structural characteristics of the 4-FTP layers do not depend on the preparation protocol (standard procedure or stepwise deposition). It thus follows that the difference between 4-CTP and 4-FTP SAMs can be primarily ascribed to the higher affinity of the CN end group to transition metals like nickel,[98] which leads to a pronounced end group−substrate interaction and molecular decomposition.

4. CONCLUSIONS

We have examined the formation of aromatic thiol SAMs on Ni(111) by vapor phase deposition. Well-defined SAMs of 4-fluorothiophenol could be grown at 200 K, bonded through the deprotonated S headgroup and with the aromatic ring forming a 60° angle to the surface. A structural model could be developed based on our comparative theoretical−experimental analysis, which indicates a coverage of $\Theta \approx 0.2$ ML in the saturated monolayer and predicts that the S atoms are coordinated in the bridge-hollow (almost on hollow) site of a basically unreconstructed Ni(111) surface layer. The thiolate-bonded SAM is only stable up to 200 K, and thermally activated cleavage of the S−C bond leads at room temperature to ill-defined monolayers that contain a considerable amount of atomic sulfur. Finally, we considered SAMs of 4-cyanothiophenol and showed that the strong interaction of the CN end group with the surface is detrimental to the growth of a densely packed layer and leads to partial decomposition of the molecules already at 200 K.

The insight gained into the nature of the Ni−thiolate bonding in this investigation demonstrates that thiolate-bonded aromatic SAMs on nickel metal substrates may pose severe stability problems close to and above room temperature, and in view of practical applications of aromatic compounds in spintronics, a search for alternative headgroups should be pursued.

■ ASSOCIATED CONTENT

Supporting Information

TPD spectra of 4-FTP and 4-CTP multilayers, additional XP multilayer spectra of both molecules, XPS comparison of the different relative coverage of 4-FTP and 4-CTP monolayers, and XP and polarization-dependent UP spectra comparing 4-FTP SAMs prepared with different procedures. The Supporting Information is available free of charge on the ACS Publications website at DOI: 10.1021/acs.jpcc.5b04351.

■ AUTHOR INFORMATION

Corresponding Authors

*E-mail: karsten.reuter@ch.tum.de.
*E-mail: francesco.allegretti@ph.tum.de.

Notes

The authors declare no competing financial interest.

■ ACKNOWLEDGMENTS

This work was supported by the Deutsche Forschungsgemeinschaft (Munich Center for Advanced Photonics, project B.1.4, and project RE1509/24-1). Financial support for synchrotron beam times was provided by the Helmholtz-Zentrum-Berlin and is gratefully acknowledged. R.H. and D.A.D. acknowledge grants from the China Scholarship Council (CSC) and Alexander von Humboldt Foundation, respectively. P.N.A. acknowledges the MINCyT (project PICT Bicentenario 1962), CONICET (project PIP 0272), and UNR (project PID 19/I375) for financial support, the CCT-Rosario Computational Center, member of the High Performance Computing National System (SNCAD, MincyT, Argentina) for allocation of computer time, and also H. F. Busnengo for helpful discussions. We also thank J. V. Barth for support and discussion, and the beamline staff at Bessy II for experimental assistance.

■ REFERENCES

(1) Ratner, M. A. Introducing Molecular Electronics. *Mater. Today* **2002**, *5*, 20−27.
(2) Love, J. C.; Estroff, L. A.; Kriebel, J. K.; Nuzzo, R. G.; Whitesides, G. M. Self-Assembled Monolayers of Thiolates on Metals as a Form of Nanotechnology. *Chem. Rev.* **2005**, *105*, 1103−1170.
(3) Newton, L.; Slater, T.; Clark, N.; Vijayaraghavan, A. Self Assembled Monolayers (SAMs) on Metallic Surfaces (Gold and Graphene) for Electronic Applications. *J. Mater. Chem. C* **2013**, *1*, 376−393.
(4) Mani, G.; Johnson, D. M.; Marton, D.; Feldman, M. D.; Patel, D.; Ayon, A. A.; Agrawal, C. M. Drug Delivery from Gold and Titanium Surfaces Using Self-Assembled Monolayers. *Biomaterials* **2008**, *29*, 4561−4573.
(5) Mastrangelo, F.; Fioravanti, G.; Quaresima, R.; Vinci, R.; Gherlone, E. Self-Assembled Monolayers (SAMs): Which Perspectives in Implant Dentistry? *J. Biomater. Nanobiotechnol.* **2011**, *2*, 533−543.
(6) Gooding, J. J.; Mearns, F.; Yang, W.; Liu, J. Self-Assembled Monolayers into the 21st Century: Recent Advances and Applications. *Electroanalysis* **2003**, *15*, 81−96.
(7) Schreiber, F. Structure and Growth of Self-Assembling Monolayers. *Prog. Surf. Sci.* **2000**, *65*, 151−257.
(8) Maksymovych, P.; Sorescu, D. C.; Yates, J. T., Jr. Gold-Adatom-Mediated Bonding in Self-Assembled Short-Chain Alkanethiolate Species on the Au(111) Surface. *Phys. Rev. Lett.* **2006**, *97*, 146103.

DOI: 10.1021/acs.jpcc.5b04351
J. Phys. Chem. C XXXX, XXX, XXX−XXX

(9) Mazzarello, R.; Cossaro, A.; Verdini, A.; Rousseau, R.; Casalis, L.; Danisman, M. F.; Floreano, L.; Scandolo, S.; Morgante, A.; Scoles, G. Structure of a CH_3S Monolayer on Au(111) Solved by the Interplay between Molecular Dynamics Calculations and Diffraction Measurements. *Phys. Rev. Lett.* **2007**, *98*, 016102.
(10) Chaudhuri, A.; Lerotholi, T. J.; Jackson, D. C.; Woodruff, D. P.; Dhanak, V. Local Methylthiolate Adsorption Geometry on Au(111) from Photoemission Core-Level Shifts. *Phys. Rev. Lett.* **2009**, *102*, 126101.
(11) Cossaro, A.; Floreano, L.; Verdini, A.; Casalis, L.; Morgante, A. Comment on "Local Methylthiolate Adsorption Geometry on Au(111) from Photoemission Core-Level Shifts. *Phys. Rev. Lett.* **2009**, *103*, 119601.
(12) Chaudhuri, A.; Lerotholi, T. J.; Jackson, D. C.; Woodruff, D. P.; Dhanak, V. Chaudhuri Et al. Reply. *Phys. Rev. Lett.* **2009**, *103*, 119602.
(13) Hakkinen, H. The Gold-Sulfur Interface at the Nanoscale. *Nat. Chem.* **2012**, *4*, 443−455.
(14) Mekhalif, Z.; Laffineur, F.; Couturier, N.; Delhalle, J. Elaboration of Self-Assembled Monolayers of n-Alkanethiols on Nickel Polycrystalline Substrates: Time, Concentration, and Solvent Effects. *Langmuir* **2003**, *19*, 637−645.
(15) Hoertz, P. G.; Niskala, J. R.; Dai, P.; Black, H. T.; You, W. Comprehensive Investigation of Self-Assembled Monolayer Formation on Ferromagnetic Thin Film Surfaces. *J. Am. Chem. Soc.* **2008**, *130*, 9763−9772.
(16) Devillers, S.; Hennart, A.; Delhalle, J.; Mekhalif, Z. 1-Dodecanethiol Self-Assembled Monolayers on Cobalt. *Langmuir* **2011**, *27*, 14849−14860.
(17) Petrovykh, D. Y.; Kimura-Suda, H.; Opdahl, A.; Richter, L. J.; Tarlov, M. J.; Whitman, L. J. Alkanethiols on Platinum: Multicomponent Self-Assembled Monolayers. *Langmuir* **2006**, *22*, 2578−2587.
(18) Love, J. C.; Wolfe, D. B.; Haasch, R.; Chabinyc, M. L.; Paul, K. E.; Whitesides, G. M.; Nuzzo, R. G. Formation and Structure of Self-Assembled Monolayers of Alkanethiolates on Palladium. *J. Am. Chem. Soc.* **2003**, *125*, 2597−2609.
(19) Fontanesi, C.; Tassinari, F.; Parenti, F.; Cohen, H.; Mondal, P. C.; Kiran, V.; Giglia, A.; Pasquali, L.; Naaman, R. New One-Step Thiol Functionalization Procedure for Ni by Self-Assembled Monolayers. *Langmuir* **2015**, *31*, 3546−3552.
(20) Emberly, E. G.; Kirczenow, G. Molecular Spintronics: Spin-Dependent Electron Transport in Molecular Wires. *Chem. Phys.* **2002**, *281*, 311−324.
(21) Xiong, Z. H.; Wu, D.; Valy Vardeny, Z.; Shi, J. Giant Magnetoresistance in Organic Spin-Valves. *Nature* **2004**, *427*, 821−824.
(22) Sanvito, S. Molecular Spintronics. *Chem. Soc. Rev.* **2011**, *40*, 3336−3355.
(23) Urdampilleta, M.; Klyatskaya, S.; Cleuziou, J. P.; Ruben, M.; Wernsdorfer, W. Supramolecular Spin Valves. *Nat. Mater.* **2011**, *10*, 502−506.
(24) Rocha, A. R.; Garcia-suarez, V. M.; Bailey, S. W.; Lambert, C. J.; Ferrer, J.; Sanvito, S. Towards Molecular Spintronics. *Nat. Mater.* **2005**, *4*, 335−339.
(25) Waldron, D.; Haney, P.; Larade, B.; MacDonald, A.; Guo, H. Nonlinear Spin Current and Magnetoresistance of Molecular Tunnel Junctions. *Phys. Rev. Lett.* **2006**, *96*, 166804.
(26) Rocha, A. R.; García-Suárez, V. M.; Bailey, S.; Lambert, C.; Ferrer, J.; Sanvito, S. Spin and Molecular Electronics in Atomically Generated Orbital Landscapes. *Phys. Rev. B* **2006**, *73*, 085414.
(27) Petta, J. R.; Slater, S. K.; Ralph, D. C. Spin-Dependent Transport in Molecular Tunnel Junctions. *Phys. Rev. Lett.* **2004**, *93*, 136601.
(28) Yamada, R.; Noguchi, M.; Tada, H. Magnetoresistance of Single Molecular Junctions Measured by a Mechanically Controllable Break Junction Method. *Appl. Phys. Lett.* **2011**, *98*, 053110.
(29) Horiguchi, K.; Sagisaka, T.; Kurokawa, S.; Sakai, A. Electron Transport through Ni/1,4-Benzenedithiol/Ni Single-Molecule Junctions under Magnetic Field. *J. Appl. Phys.* **2013**, *113*, 144313.
(30) Barraud, C.; Seneor, P.; Mattana, R.; Fusil, S.; Bouzehouane, K.; Deranlot, C.; Graziosi, P.; Hueso, L.; Bergenti, I.; Dediu, V.; et al. Unravelling the Role of the Interface for Spin Injection into Organic Semiconductors. *Nat. Phys.* **2010**, *6*, 615−620.
(31) Sanvito, S. Molecular Spintronics: The Rise of Spinterface Science. *Nat. Phys.* **2010**, *6*, 562−564.
(32) Kämper, K. P.; Schmitt, W.; Wesner, D. A.; Güntherodt, G. Thickness Dependence of the Spin- and Angle-Resolved Photoemission of Ultrathin, Epitaxial Ni(111)/W(110) Layers. *Appl. Phys. A: Mater. Sci. Process.* **1989**, *49*, 573−578.
(33) Li, Y.; Farle, M.; Baberschke, K. Critical Spin Fluctuations and Curie Temperatures of Ultrathin Ni(111)/W(110): A Magnetic-Resonance Study in Ultrahigh Vacuum. *Phys. Rev. B* **1990**, *41*, 9596−9599.
(34) Wan, L.-J.; Terashima, M.; Noda, H.; Osawa, M. Molecular Orientation and Ordered Structure of Benzenethiol Adsorbed on Gold(111). *J. Phys. Chem. B* **2000**, *104*, 3563−3569.
(35) Wang, L.; Liu, L.; Chen, W.; Feng, Y.; Wee, A. T. S. Configuration-Dependent Interface Charge Transfer at a Molecule−Metal Junction. *J. Am. Chem. Soc.* **2006**, *128*, 8003−8007.
(36) Chen, W.; Wee, A. T. S. Synchrotron PES and NEXAFS Studies of Self-Assembled Aromatic Thiol Monolayers on Au(111). *J. Electron Spectrosc. Relat. Phenom.* **2009**, *172*, 54−63.
(37) Jiang, P.; Deng, K.; Fichou, D.; Xie, S.-S.; Nion, A.; Wang, C. Stm Imaging Ortho- and Para-Fluorothiophenol Self-Assembled Monolayers on Au(111). *Langmuir* **2009**, *25*, 5012−5017.
(38) Hamoudi, H.; Neppl, S.; Kao, P.; Schüpbach, B.; Feulner, P.; Terfort, A.; Allara, D.; Zharnikov, M. Orbital-Dependent Charge Transfer Dynamics in Conjugated Self-Assembled Monolayers. *Phys. Rev. Lett.* **2011**, *107*, 027801.
(39) Hamoudi, H.; Kao, P.; Nefedov, A.; Allara, D. L.; Zharnikov, M. X-Ray Spectroscopy Characterization of Self-Assembled Monolayers of Nitrile-Substituted Oligo(Phenylene Ethynylene)S with Variable Chain Length. *Beilstein J. Nanotechnol.* **2012**, *3*, 12−24.
(40) Wong, K. L.; Lin, X.; Kwon, K. Y.; Pawin, G.; Rao, B. V.; Liu, A.; Bartels, L.; Stolbov, S.; Rahman, T. S. Halogen-Substituted Thiophenol Molecules on Cu(111). *Langmuir* **2004**, *20*, 10928−10934.
(41) Di Castro, V.; Bussolotti, F.; Mariani, C. The Evolution of Benzenethiol Self-Assembled Monolayer on the Cu(100) Surface. *Surf. Sci.* **2005**, *598*, 218−225.
(42) Allegretti, F.; Bussolotti, F.; Woodruff, D. P.; Dhanak, V. R.; Beccari, M.; Di Castro, V.; Betti, M. G.; Mariani, C. The Local Adsorption Geometry of Benzenethiolate on Cu(100). *Surf. Sci.* **2008**, *602*, 2453−2462.
(43) Schmidt, C.; Götzen, J.; Witte, G. Temporal Evolution of Benzenethiolate SAMs on Cu(100). *Langmuir* **2011**, *27*, 1025−1032.
(44) Schmidt, C.; Witt, A.; Witte, G. Tailoring the Cu(100) Work Function by Substituted Benzenethiolate Self-Assembled Monolayers. *J. Phys. Chem. A* **2011**, *115*, 7234−7241.
(45) Dannenberger, O.; Weiss, K.; Himmel, H. J.; Jäger, B.; Buck, M.; Wöll, C. An Orientation Analysis of Differently Endgroup-Functionalised Alkanethiols Adsorbed on Au Substrates. *Thin Solid Films* **1997**, *307*, 183−191.
(46) Woodruff, D. P.; Delchar, T. A. *Modern Techniques of Surface Science*; Cambridge University Press: Cambridge, U.K., 2008.
(47) Blobner, F.; Neppl, S.; Feulner, P. A Versatile Partial Electron Yield Detector with Large Acceptance Angle and Well-Defined Threshold Energy and Gain. *J. Electron Spectrosc. Relat. Phenom.* **2011**, *184*, 483−486.
(48) Stöhr, J. *NEXAFS Spectroscopy*; Springer-Verlag: Berlin, Germany, 2003.
(49) Feulner, P.; Niedermayer, T.; Eberle, K.; Schneider, R.; Menzel, D.; Baumer, A.; Schmich, E.; Shaporenko, A.; Tai, Y.; Zharnikov, M. Strong Temperature Dependence of Irradiation Effects in Organic Layers. *Phys. Rev. Lett.* **2004**, *93*, 178302.
(50) Shaporenko, A.; Zharnikov, M.; Feulner, P.; Menzel, D. Quantitative Analysis of Temperature Effects in Radiation Damage

DOI: 10.1021/acs.jpcc.5b04351
J. Phys. Chem. C XXXX, XXX, XXX−XXX

of Thiolate-Based Self-Assembled Monolayers. *J. Phys.: Condens. Matter* **2006**, *18*, S1677.
(51) Kresse, G.; Furthmüller, J. Efficiency of *Ab-Initio* Total Energy Calculations for Metals and Semiconductors Using a Plane-Wave Basis Set. *Comput. Mater. Sci.* **1996**, *6*, 15−50.
(52) Kresse, G.; Furthmüller, J. Efficient Iterative Schemes for *Ab Initio* Total-Energy Calculations Using a Plane-Wave Basis Set. *Phys. Rev. B* **1996**, *54*, 11169−11186.
(53) Clark, S. J.; Segal, M. D.; Pickard, C. J.; Hasnip, P. J.; Probert, M. I. J.; Refson, K.; Payne, M. C. First Principles Methods Using CASTEP. *Z. Kristallogr.* **2005**, *220*, 567−570.
(54) Kohn, W.; Sham, L. J. Self-Consistent Equations Including Exchange and Correlation Effects. *Phys. Rev.* **1965**, *140*, A1133−A1138.
(55) Perdew, J. P.; Burke, K.; Ernzerhof, M. Generalized Gradient Approximation Made Simple. *Phys. Rev. Lett.* **1996**, *77*, 3865−3868.
(56) Ruiz, V. G.; Liu, W.; Zojer, E.; Scheffler, M.; Tkatchenko, A. Density-Functional Theory with Screened Van der Waals Interactions for the Modeling of Hybrid Inorganic-Organic Systems. *Phys. Rev. Lett.* **2012**, *108*, 146103.
(57) Monkhorst, H. J.; Pack, J. D. Special Points for Brillouin-Zone Integrations. *Phys. Rev. B* **1976**, *13*, 5188−5192.
(58) Gao, S.-P.; Pickard, C. J.; Payne, M. C.; Zhu, J.; Yuan, J. Theory of Core-Hole Effects in *1s* Core-Level Spectroscopy of the First-Row Elements. *Phys. Rev. B* **2008**, *77*, 115122.
(59) Shang-Peng, G.; Chris, J. P.; Alexander, P.; Victor, M. Core-Level Spectroscopy Calculation and the Plane Wave Pseudopotential Method. *J. Phys.: Condens. Matter* **2009**, *21*, 104203.
(60) Kolczewski, C.; Williams, F. J.; Cropley, R. L.; Vaughan, O. P. H.; Urquhart, A. J.; Tikhov, M. S.; Lambert, R. M.; Hermann, K. Adsorption Geometry and Core Excitation Spectra of Three Phenylpropene Isomers on Cu(111). *J. Chem. Phys.* **2006**, *125*, 034701.
(61) Laibinis, P. E.; Whitesides, G. M.; Allara, D. L.; Tao, Y. T.; Parikh, A. N.; Nuzzo, R. G. Comparison of the Structures and Wetting Properties of Self-Assembled Monolayers of n-Alkanethiols on the Coinage Metal Surfaces, Copper, Silver, and Gold. *J. Am. Chem. Soc.* **1991**, *113*, 7152−7167.
(62) Rufael, T. S.; Huntley, D. R.; Mullins, D. R.; Gland, J. L. Adsorption and Reactions of Benzenethiol on the Ni(111) Surface. *J. Phys. Chem.* **1994**, *98*, 13022−13027.
(63) Rufael, T. S.; Huntley, D. R.; Mullins, D. R.; Gland, J. L. Adsorption and Reaction of Dimethyl Disulfide on the Ni(111) Surface. *J. Phys. Chem. B* **1998**, *102*, 3431−3440.
(64) Mullins, D. R.; Huntley, D. R.; Overbury, S. H. The Nature of the Sulfur Induced Surface Reconstruction on Ni(111). *Surf. Sci.* **1995**, *323*, L287−L292.
(65) Rufael, T. S.; Huntley, D. R.; Mullins, D. R.; Gland, J. L. Methyl Thiolate on Ni(111): Multiple Adsorption Sites and Mechanistic Implications. *J. Phys. Chem.* **1995**, *99*, 11472−11480.
(66) Ishida, T.; Hara, M.; Kojima, I.; Tsuneda, S.; Nishida, N.; Sasabe, H.; Knoll, W. High Resolution X-Ray Photoelectron Spectroscopy Measurements of Octadecanethiol Self-Assembled Monolayers on Au(111). *Langmuir* **1998**, *14*, 2092−2096.
(67) Takiguchi, H.; Sato, K.; Ishida, T.; Abe, K.; Yase, K.; Tamada, K. Delicate Surface Reaction of Dialkyl Sulfide Self-Assembled Monolayers on Au(111). *Langmuir* **1999**, *16*, 1703−1710.
(68) Heister, K.; Rong, H. T.; Buck, M.; Zharnikov, M.; Grunze, M.; Johansson, L. S. O. Odd−Even Effects at the S-Metal Interface and in the Aromatic Matrix of Biphenyl-Substituted Alkanethiol Self-Assembled Monolayers. *J. Phys. Chem. B* **2001**, *105*, 6888−6894.
(69) Shaporenko, A.; Terfort, A.; Grunze, M.; Zharnikov, M. A Detailed Analysis of the Photoemission Spectra of Basic Thioaromatic Monolayers on Noble Metal Substrates. *J. Electron Spectrosc. Relat. Phenom.* **2006**, *151*, 45−51.
(70) Castner, D. G.; Hinds, K.; Grainger, D. W. X-Ray Photoelectron Spectroscopy Sulfur 2p Study of Organic Thiol and Disulfide Binding Interactions with Gold Surfaces. *Langmuir* **1996**, *12*, 5083−5086.
(71) Noh, J.; Ito, E.; Hara, M. Self-Assembled Monolayers of Benzenethiol and Benzenemethanethiol on Au(111): Influence of an Alkyl Spacer on the Structure and Thermal Desorption Behavior. *J. Colloid Interface Sci.* **2010**, *342*, 513−517.
(72) Klekamp, A.; Umbach, E. Photon-Induced Dissociation of Physisorbed SF_6 on Ni(111). *Chem. Phys. Lett.* **1990**, *171*, 233−238.
(73) Ulman, A. Formation and Structure of Self-Assembled Monolayers. *Chem. Rev.* **1996**, *96*, 1533−1554.
(74) Stettner, J.; Winkler, A. Characterization of Alkanethiol Self-Assembled Monolayers on Gold by Thermal Desorption Spectroscopy. *Langmuir* **2010**, *26*, 9659−9665.
(75) Stammer, X.; Tonigold, K.; Bashir, A.; Kafer, D.; Shekhah, O.; Hulsbusch, C.; Kind, M.; Gro; Woll, C. A Highly Ordered, Aromatic Bidentate Self-Assembled Monolayer on Au(111): A Combined Experimental and Theoretical Study. *Phys. Chem. Chem. Phys.* **2010**, *12*, 6445−6454.
(76) Vericat, C.; Vela, M. E.; Corthey, G.; Pensa, E.; Cortes, E.; Fonticelli, M. H.; Ibanez, F.; Benitez, G. E.; Carro, P.; Salvarezza, R. C. Self-Assembled Monolayers of Thiolates on Metals: A Review Article on Sulfur-Metal Chemistry and Surface Structures. *RSC Adv.* **2014**, *4*, 27730−27754.
(77) Mullins, D. R.; Huntley, D. R.; Tang, T.; Saldin, D. K.; Tysoe, W. T. The Adsorption Site and Orientation of CH_3S on Ni(111). *Surf. Sci.* **1997**, *380*, 468−480.
(78) Fisher, C. J.; Woodruff, D. P.; Jones, R. G.; Cowie, B. C. C.; Formoso, V. Chemical-Shift X-Ray Standing Wavefield Determination of the Local Structure of Methanethiolate Phases on Ni(111). *Surf. Sci.* **2002**, *496*, 73−86.
(79) Kane, S. M.; Gland, J. L. Cyclohexanethiol Adsorption and Reaction on the Ni(111) Surface. *J. Phys. Chem. B* **1998**, *102*, 5322−5328.
(80) Mekhalif, Z.; Riga, J.; Pireaux, J. J.; Delhalle, J. Self-Assembled Monolayers of n-Dodecanethiol on Electrochemically Modified Polycrystalline Nickel Surfaces. *Langmuir* **1997**, *13*, 2285−2290.
(81) Bengió, S.; Fonticelli, M.; Benítez, G.; Creus, A. H.; Carro, P.; Ascolani, H.; Zampieri, G.; Blum, B.; Salvarezza, R. C. Electrochemical Self-Assembly of Alkanethiolate Molecules on Ni(111) and Polycrystalline Ni Surfaces. *J. Phys. Chem. B* **2005**, *109*, 23450−23460.
(82) Sadler, J. E.; Szumski, D. S.; Kierzkowska, A.; Catarelli, S. R.; Stella, K.; Nichols, R. J.; Fonticelli, M. H.; Benitez, G.; Blum, B.; Salvarezza, R. C.; et al. Surface Functionalization of Electro-Deposited Nickel. *Phys. Chem. Chem. Phys.* **2011**, *13*, 17987−17993.
(83) Rajalingam, S.; Devillers, S.; Dehalle, J.; Mekhalif, Z. A Two Step Process to Form Organothiol Self-Assembled Monolayers on Nickel Surfaces. *Thin Solid Films* **2012**, *522*, 247−253.
(84) Thompson, A.; Attwood, D.; Gullikson, E.; Howells, M.; Kim, K.-J.; Kirz, J.; Kortright, J.; Lindau, I.; Liu, Y.; Pianetta, P.; et al. *X-Ray Data Booklet*, 3rd ed.; Lawrence Berkeley National Laboratory and University of California: Berkeley, CA, 2009.
(85) Cavalleri, O.; Gonella, G.; Terreni, S.; Vignolo, M.; Pelori, P.; Floreano, L.; Morgante, A.; Canepa, M.; Rolandi, R. High Resolution XPS of the S 2p Core Level Region of the L-Cysteine/Gold Interface. *J. Phys.: Condens. Matter* **2004**, *16*, S2477.
(86) Based on the energy difference between high symmetry adsorption sites, estimated diffusion barriers are 0.03, 0.11, 0.14, and 0.29 eV for thiol, thiolate, H, and S, respectively.
(87) From the experimental point of view, this is in line with the appearance of a faint (2 × 2) LEED pattern after prolonged annealing of the SAM slightly above 200 K, when accumulation of atomic sulfur takes place as indicated by XPS. This signals that patches with the low-coverage phase of S/Ni(111), $\Theta \approx 0.25$ ML (ref 64), become locally present.
(88) Kao, P.; Neppl, S.; Feulner, P.; Allara, D. L.; Zharnikov, M. Charge Transfer Time in Alkanethiolate Self-Assembled Monolayers via Resonant Auger Electron Spectroscopy. *J. Phys. Chem. C* **2010**, *114*, 13766−13773.
(89) Nakayama, T.; Inamura, K.; Inoue, Y.; Ikeda, S.; Kishi, K. Adsorption of Benzonitrile and Alkyl Cyanides on Evaporated Nickel and Palladium Films Studied by XPS. *Surf. Sci.* **1987**, *179*, 47−58.

DOI: 10.1021/acs.jpcc.5b04351
J. Phys. Chem. C XXXX, XXX, XXX−XXX

(90) This conclusion is reinforced by the binding energy shift of −0.75 eV for the centroid of the C 1s spectrum relative to the multilayer, cf. Figure 10b and Figure S4.
(91) Kishi, K.; Okino, Y.; Fujimoto, Y. XPS Studies of the Adsorption of CH_3CN and C_6H_5CN on the Ni(111) Surface. *Surf. Sci.* **1986**, *176*, 23−31.
(92) Gouttebaron, R.; Bourgeois, S.; Perdereau, M. Study by Static Sims, XPS and UPS of the Adsorption of Cyanogen on (100) Ni Surfaces. *Surf. Sci.* **2000**, *458*, 239−246.
(93) Rao, C. N. R.; Ranga Rao, G. Nature of Nitrogen Adsorbed on Transition Metal Surfaces as Revealed by Electron Spectroscopy and Cognate Techniques. *Surf. Sci. Rep.* **1991**, *13*, 223−263.
(94) Nilsson, A.; Mårtensson, N. Core-Level Shake-up Spectra from Ordered C, N and O Overlayers on Ni(100). *Chem. Phys. Lett.* **1991**, *182*, 147−151.
(95) Chorkendorff, I.; Russell, J. N.; Yates, J. T. Surface Reaction Pathways of Methylamine on the Ni(111) Surface. *J. Chem. Phys.* **1987**, *86*, 4692−4700.
(96) Hagans, P. L.; Chorkendorff, I.; Yates, J. T. Scanning Kinetic Spectroscopy and Temperature-Programmed Desorption Studies of the Adsorption and Decomposition of Hydrogen Cyanide on the Nickel(111) Surface. *J. Phys. Chem.* **1988**, *92*, 471−476.
(97) Myers, A. K.; Benziger, J. B. Effect of Substituent Groups on the Interaction of Benzene with Nickel(111). *Langmuir* **1989**, *5*, 1270−1288.
(98) Nakao, Y.; Hiyama, T. Nickel-Catalyzed Carbocyanation of Alkynes. *Pure Appl. Chem.* **2008**, *80*, 1097−1107.

DOI: 10.1021/acs.jpcc.5b04351
J. Phys. Chem. C XXXX, XXX, XXX−XXX